

Figure 4-1. Diagram of a Zn-Cu electrochemical cell. Zn and Cu metal electrodes are immersed in a CuSO₄ solution. Electrons flow from left to right and a potential is recorded by the voltmeter. With time, this potential decreases to zero, the concentration of Zn²⁺ increases in the left-hand half of the cell, and the concentration of Cu²⁺ decreases in the right-hand half of the cell. After Faure (1998).

Table 4-1. Oxidation-reduction reactions

Reaction	ΔG_R° (kJ mol ⁻¹)
$\text{Zn} + \text{Fe}^{2+} \rightleftharpoons \text{Zn}^{2+} + \text{Fe}$	-68.4
$\text{Fe} + \text{Cu}^{2+} \rightleftharpoons \text{Fe}^{2+} + \text{Cu}$	-144.4
$\text{Cu} + 2\text{Ag}^+ \rightleftharpoons \text{Cu}^{2+} + 2\text{Ag}$	-88.7

Table 4-2. Electromotive series for selected half-reactions arranged in order of decreasing strengths as reducing agents

Oxidizing agent			Reducing agent	Standard electrode potential, V
Li ⁺	+1e ⁻	→	Li	-3.045
Na ⁺	+1e ⁻	→	Na	-2.714
Pu ³⁺	+3e ⁻	→	Pu	-2.07
Th ⁴⁺	+4e ⁻	→	Th	-1.90
Np ³⁺	+3e ⁻	→	Np	-1.86
Al ³⁺	+3e ⁻	→	Al	-1.66
U ⁴⁺	+4e ⁻	→	U	-1.38
Mn ²⁺	+2e ⁻	→	Mn	-1.18
V ³⁺	+3e ⁻	→	V	-0.87
Zn ²⁺	+2e ⁻	→	Zn	-0.763
S	+2e ⁻	→	S ²⁻	-0.44
Fe ²⁺	+2e ⁻	→	Fe	-0.41
Cd ²⁺	+2e ⁻	→	Cd	-0.403
Co ²⁺	+2e ⁻	→	Co	-0.277
Ni ²⁺	+2e ⁻	→	Ni	-0.250
Sn ²⁺	+2e ⁻	→	Sn	-0.140
Pb ²⁺	+2e ⁻	→	Pb	-0.126
2H ⁺	+2e ⁻	→	H ₂	0.00
Ti ⁴⁺	+1e ⁻	→	Ti ³⁺	0.04
Sn ⁴⁺	+2e ⁻	→	Sn ²⁺	0.15
Cu ²⁺	+2e ⁻	→	Cu	0.337
Cu ⁺	+1e ⁻	→	Cu	0.521
Se	+2e ⁻	→	Se ²⁻	0.67
Fe ³⁺	+1e ⁻	→	Fe ²⁺	0.771
Ag ⁺	+1e ⁻	→	Ag	0.799
Pu ⁴⁺	+1e ⁻	→	Pu ³⁺	0.97
Au ³⁺	+3e ⁻	→	Au	1.50
Co ³⁺	+1e ⁻	→	Co ²⁺	1.82

Figure 4-2. Stability limits for natural waters at the earth's surface in terms of Eh and pH at 25°C. The limits are based on partial pressures of oxygen of 1 and $10^{-83.1}$ atm. Also shown is the emf in *pe* units. The range of Eh and pH conditions for various natural environments is modified from Garrels and Christ (1965.)

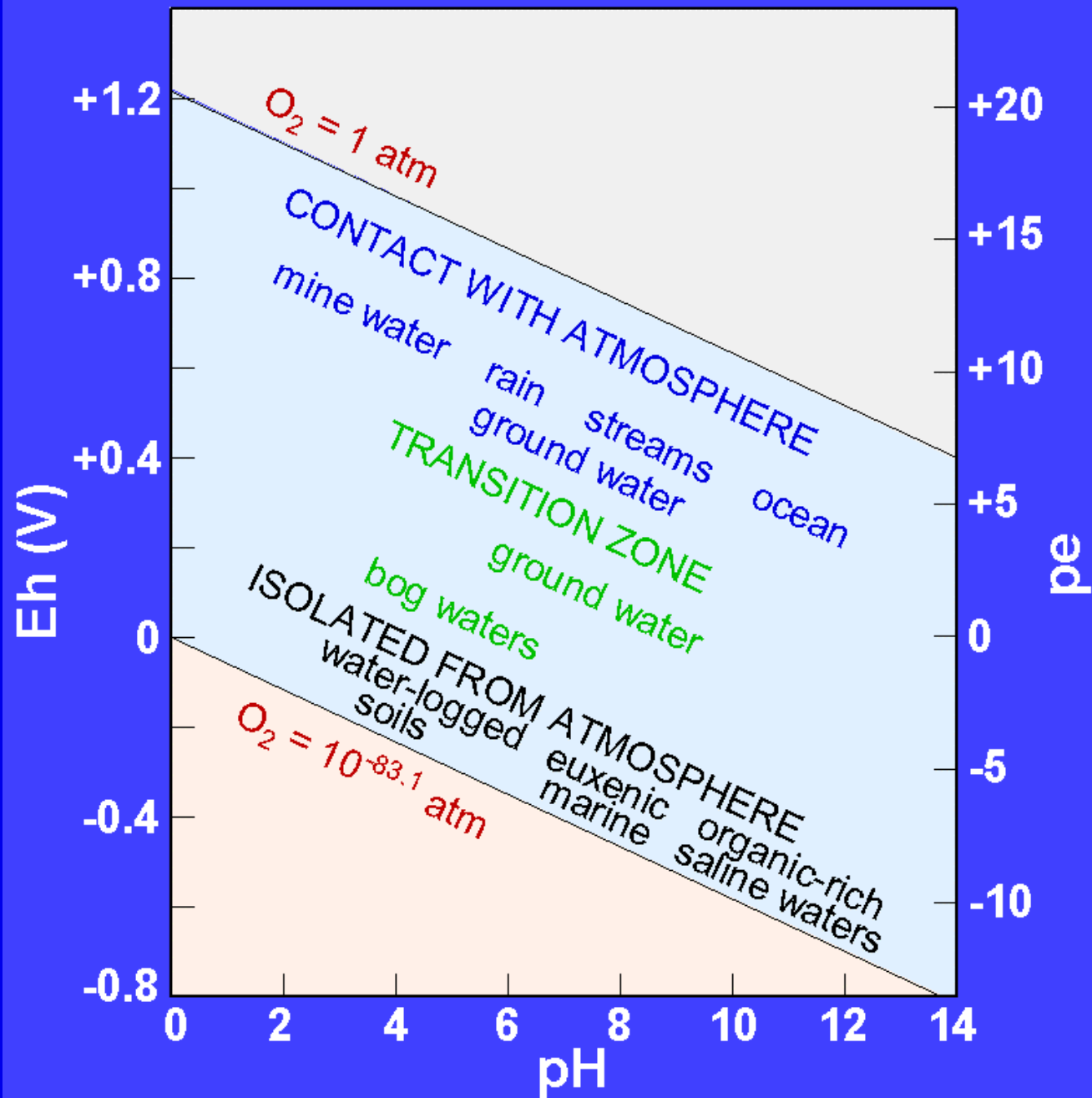


Figure 4-3. Eh-pH diagram showing the stability limits of hematite, magnetite, and metallic iron at 25°C in the presence of water.

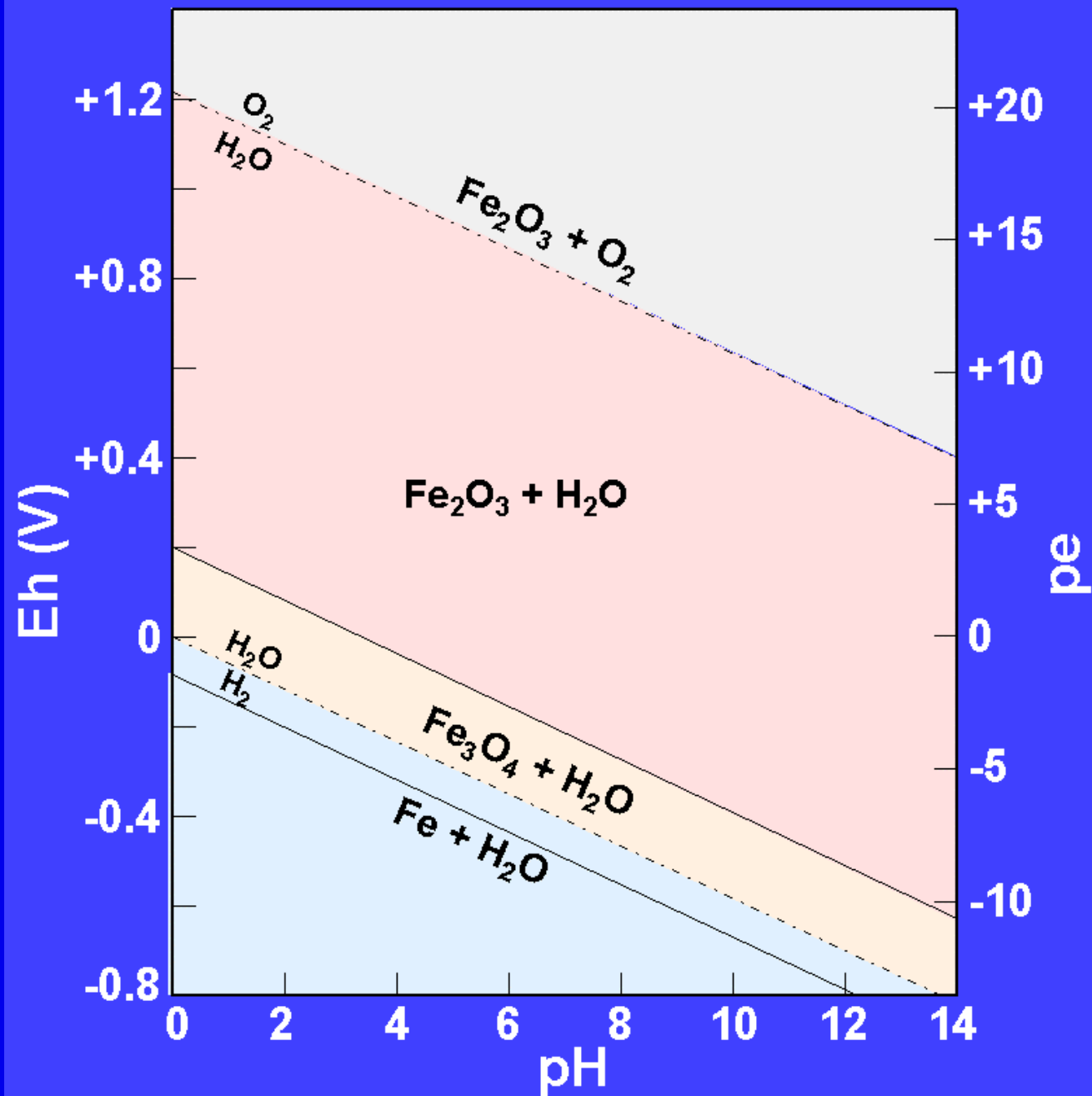


Figure 4-4. Eh-pH diagram showing variation in $[\text{Fe}^{3+}]$, in mol L^{-1} , for a solution coexisting with hematite or magnetite. Only at very low pH values does Fe^{3+} have a significant activity.

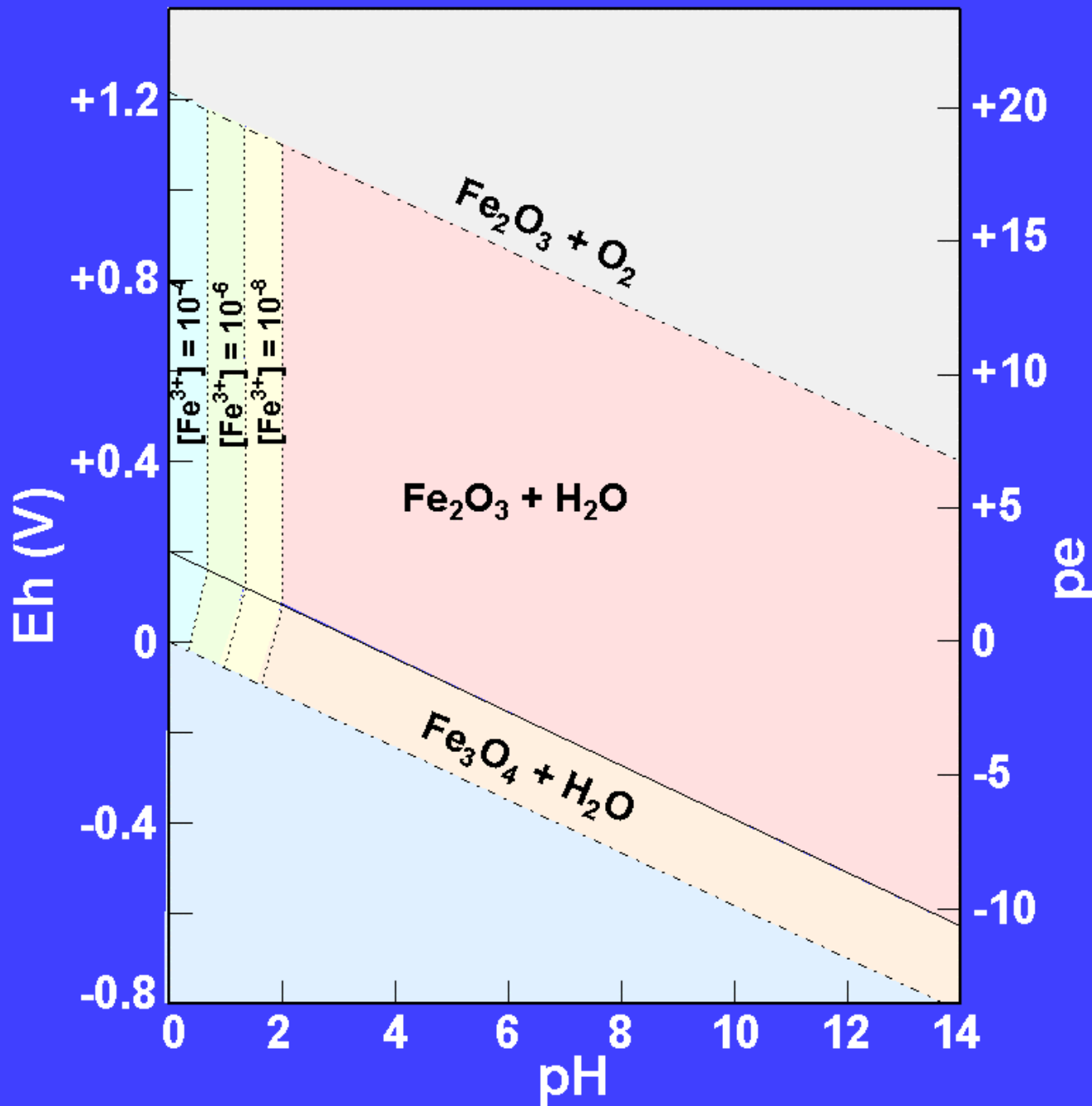


Figure 4-5. Eh-pH diagram showing the variation in $[\text{Fe}^{2+}]$, in mol L^{-1} , for a solution coexisting with hematite or magnetite. The arrow indicates increasing oxidation. See text for discussion.

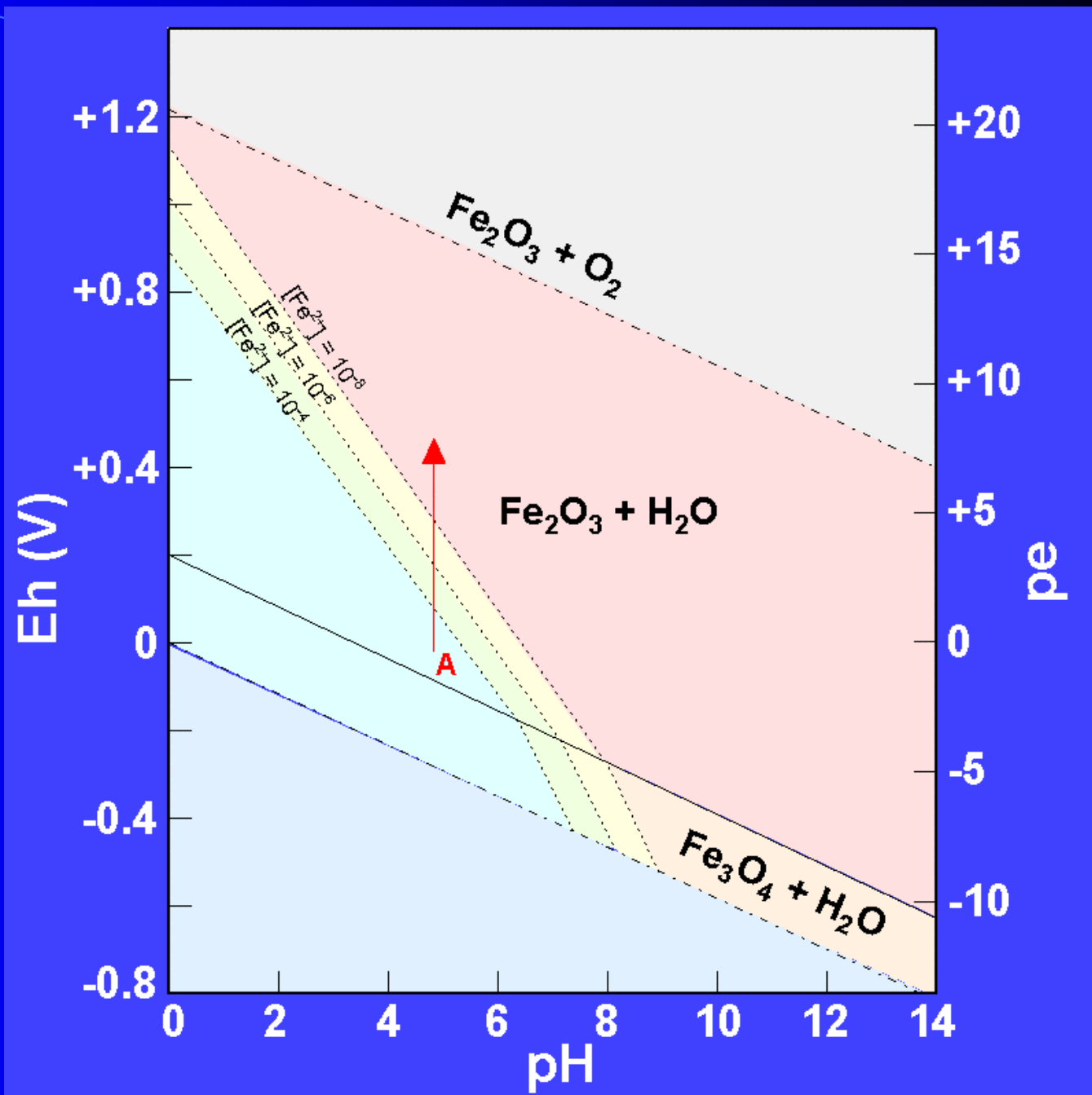


Figure 4-6. Composite diagram showing the stability fields for hematite and magnetite as a function of Eh and pH. The boundary for the ionic species is drawn with activity = 10^{-6} mol L^{-1} . In the field labeled Fe^{2+} , $[Fe^{2+}] > [Fe^{3+}]$. In the field labeled Fe^{3+} , $[Fe^{3+}] > [Fe^{2+}]$. For a system containing hematite or magnetite, the solution is in equilibrium with the solid phase.

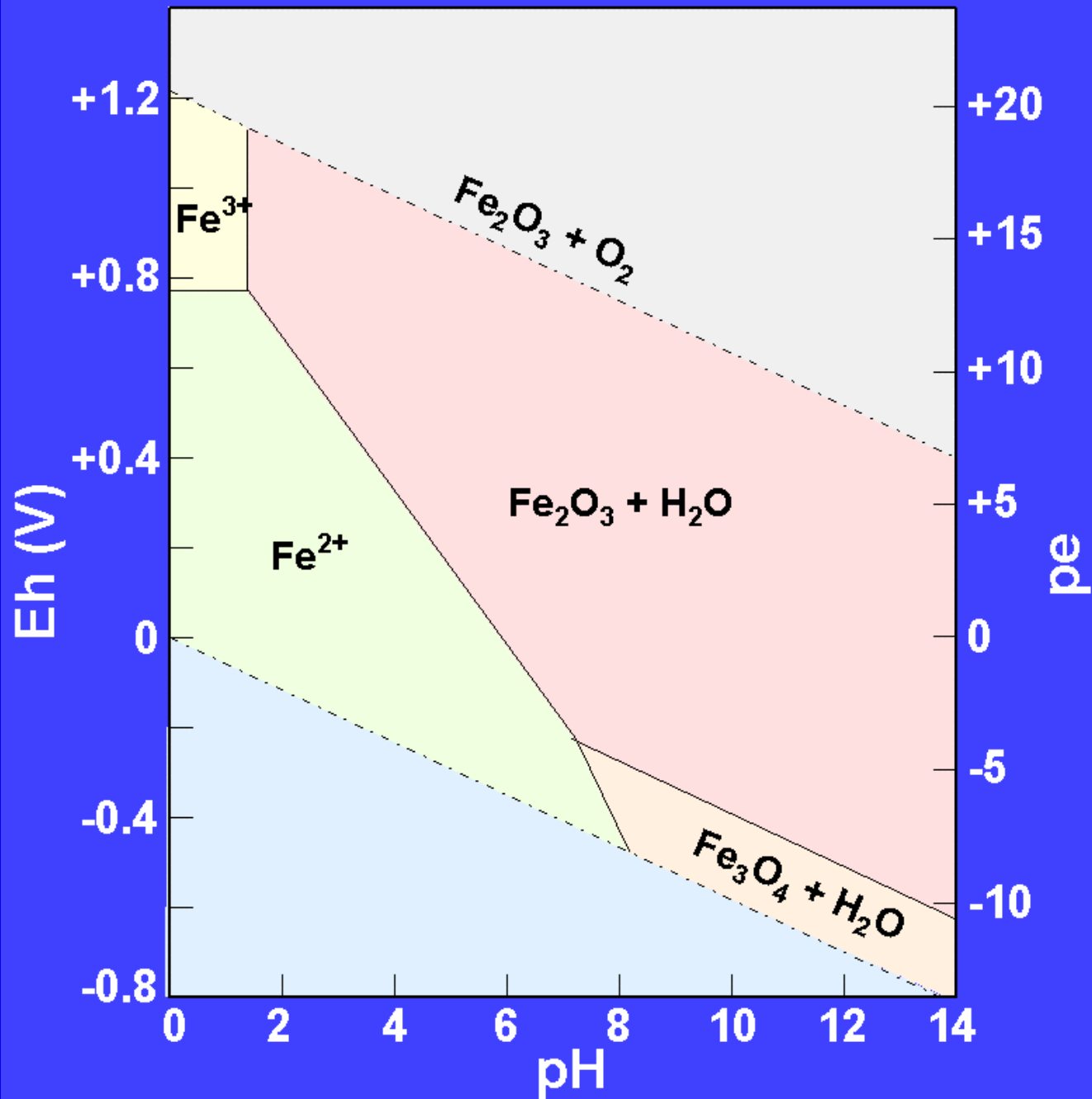


Figure 4-7. Composite Eh-pH diagram showing the stability fields of hematite, magnetite, and siderite as a function of Eh and pH. For ionic species, activity = 10^{-6} mol L⁻¹. $P_{\text{CO}_2} = 10^{-2}$ atm, a partial pressure greater than that of the earth's atmosphere. At $P_{\text{CO}_2} = 10^{-3.5}$ atm, the actual partial pressure, siderite would plot below the stability limit of liquid H₂O.

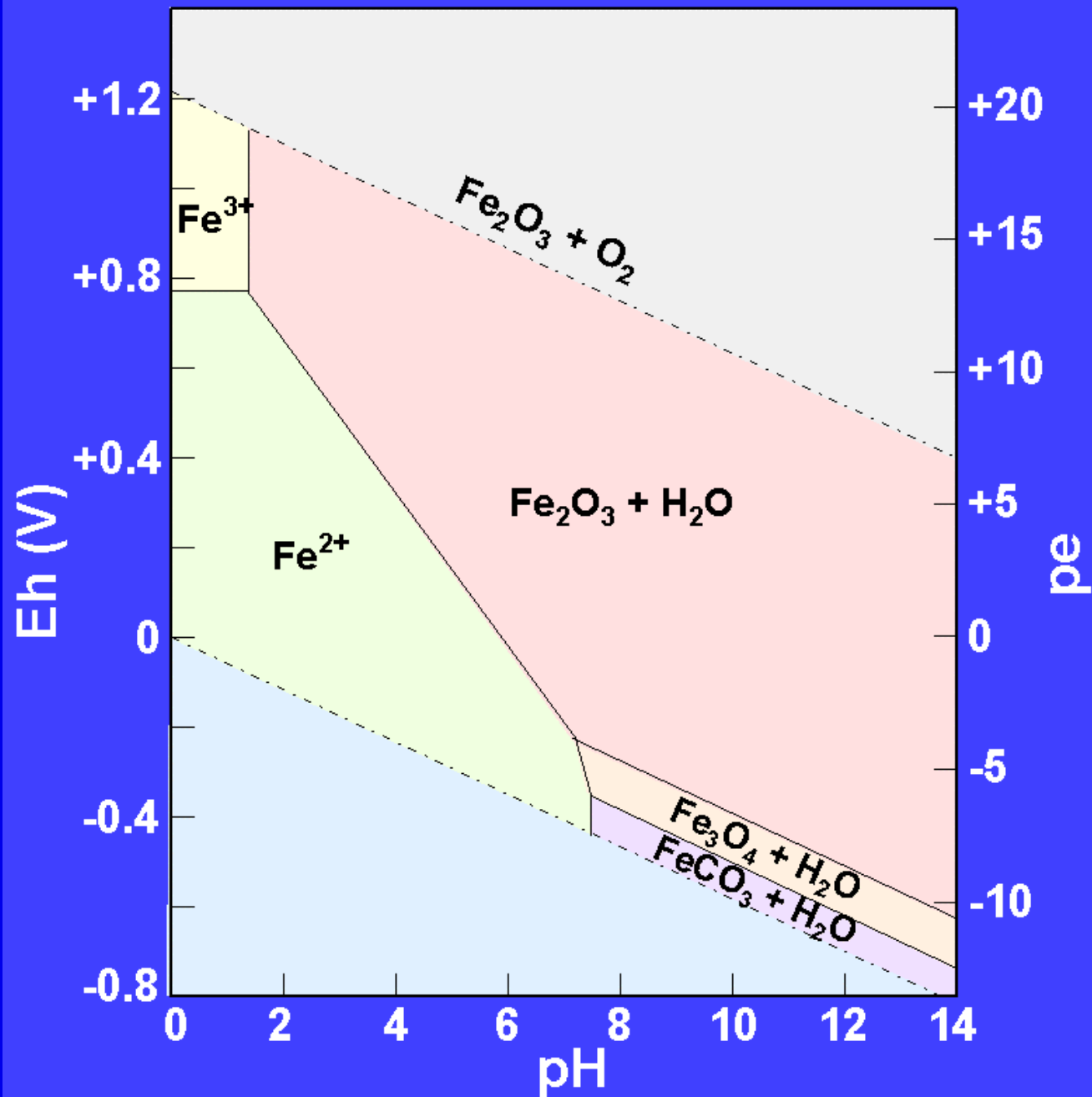


Figure 4-8. Composite Eh-pH diagram showing the stability relations for the iron oxides, carbonates, and sulfides in water at 25°C. Activity of Fe species = 1×10^{-6} mol L⁻¹, total dissolved carbonate = 1 mol L⁻¹, and total dissolved sulfur = 1×10^{-6} mol L⁻¹. After Garrels and Christ (1965).

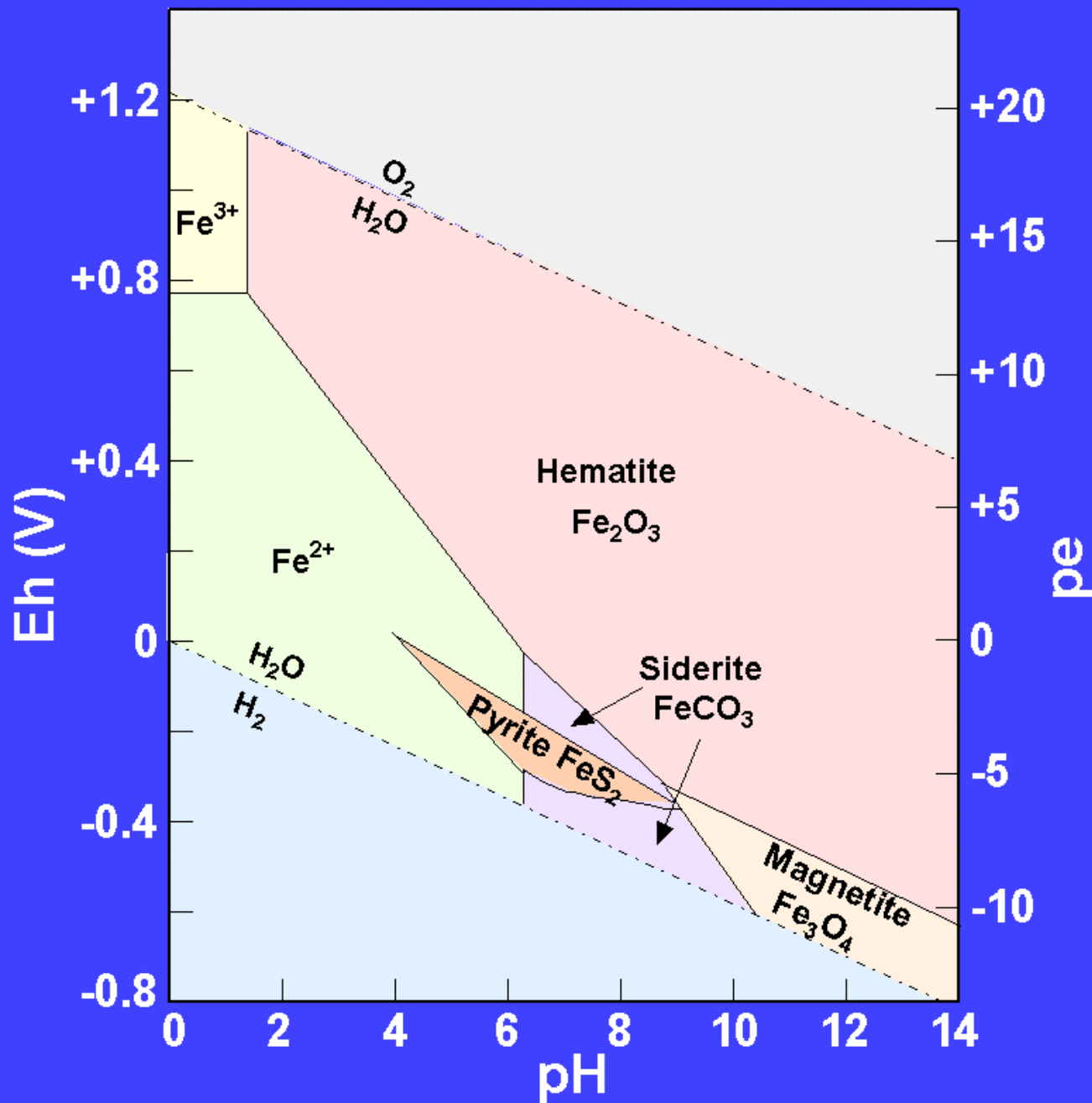


Figure 4-9. Eh-pH diagram for the nitrogen system at 25°C. $N_2 = 0.77$ atm and activity of the dissolved species = 10^{-3} mol L⁻¹. The dashed lines indicate the boundary between NO_3^- and NO_2^- for activity ratios of 1 and 10^4 . Because N_2 is a more reduced form of nitrogen, NO_2^- must exist metastably in this region. Only at very low concentrations of NO_2^- would it be the stable species relative to N_2 .

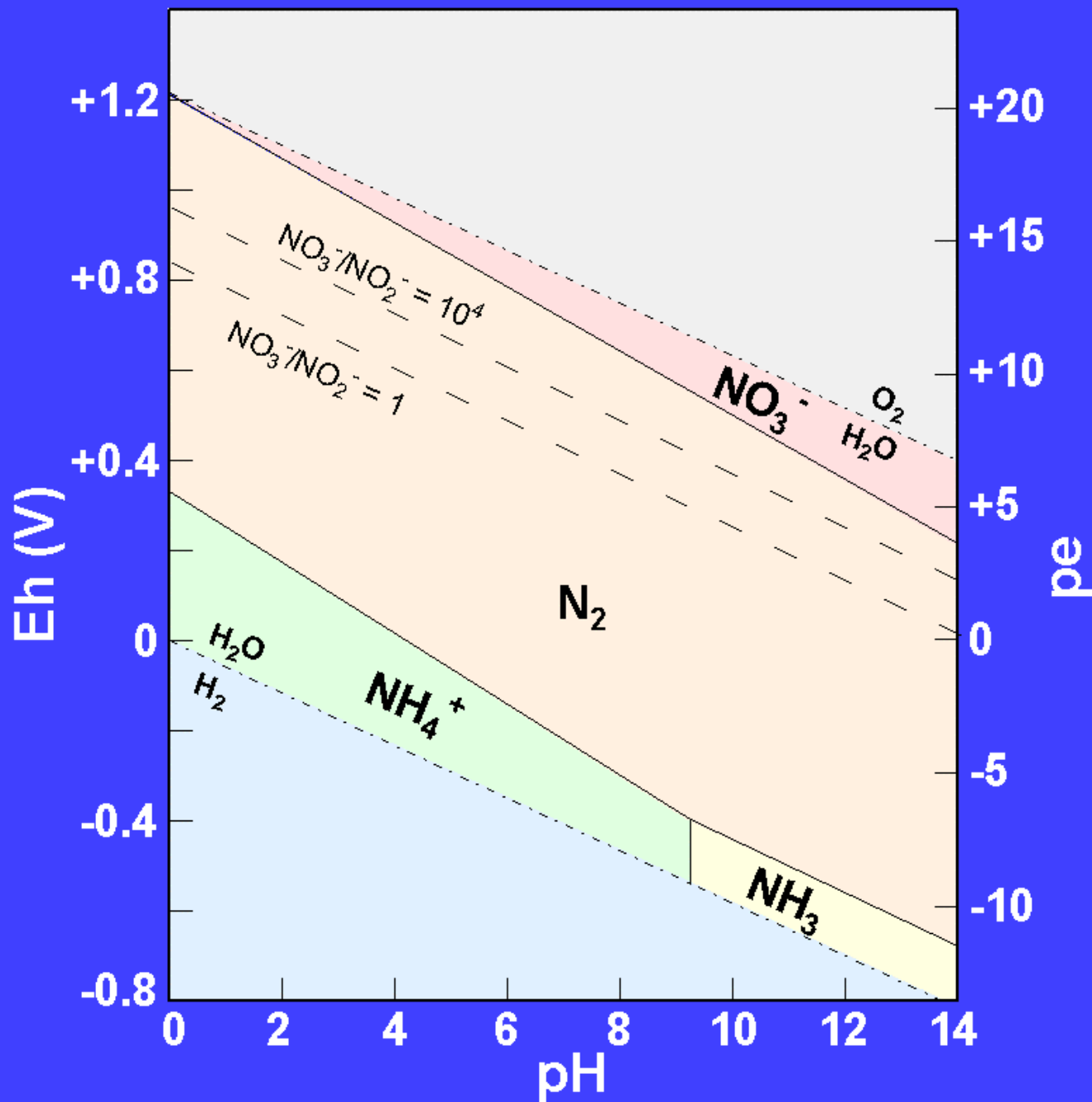
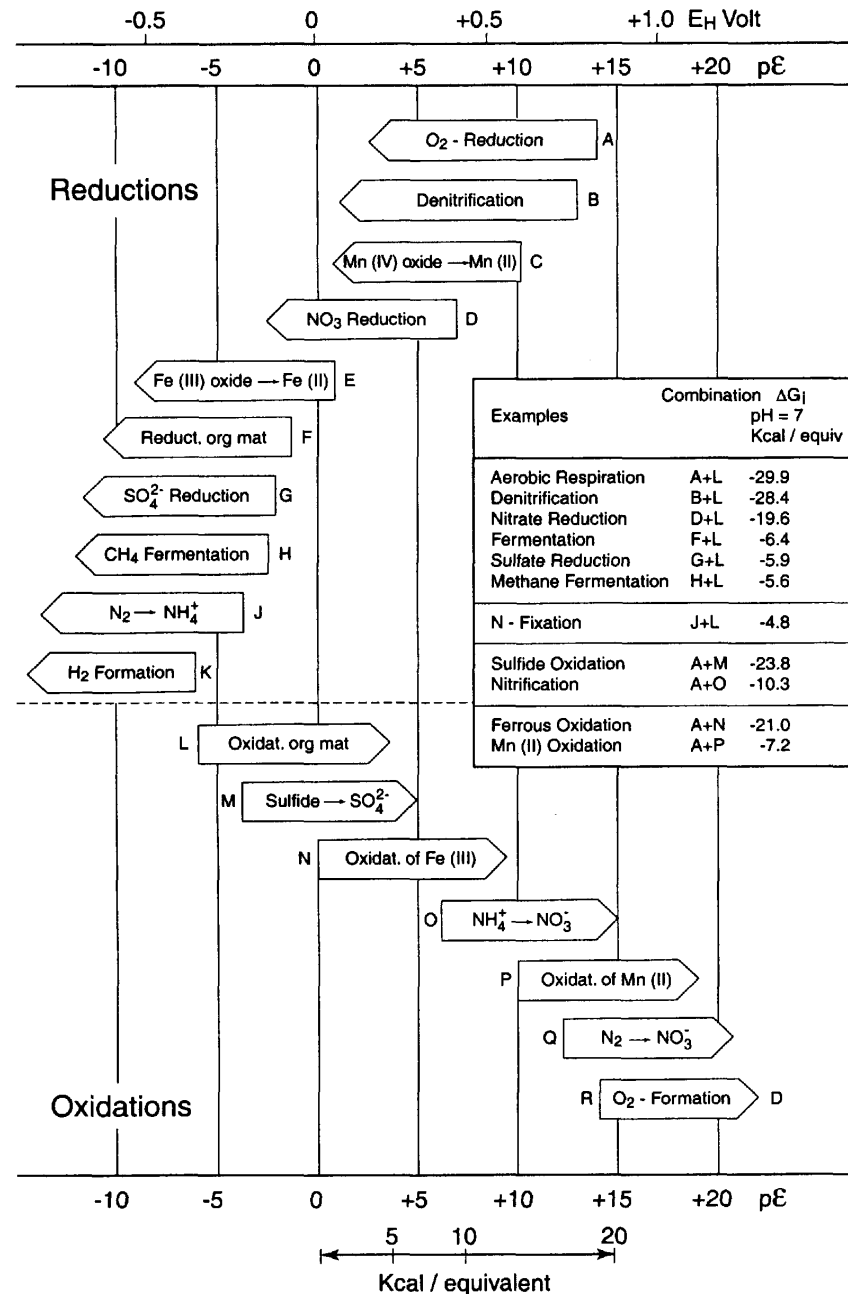


Table 4-3. Reduction and oxidation reactions that may be combined to produce biologically mediated redox reactions

Reduction		Oxidation	
A	$O_2 (g) + 4H^+ + e^- \rightarrow 2H_2O$	L	$CH_2O (aq) + H_2O \rightarrow CO_2 (g) + 4H^+ + 4e^-$
B	$2NO_3^- + 12H^+ + 10e^- \rightarrow N_2 (g) + 6H_2O$	L-1	$HCOO^- \rightarrow CO_2 (g) + H^+ + 2e^-$
C	$MnO_2 (s) + HCO_3^- + 3H^+ + 2e^- \rightarrow MnCO_3 (s) + 2H_2O$	L-2	$CH_2O (aq) + H_2O \rightarrow HCOO^- + 3H^+ + 2e^-$
D	$NO_3^- + 10H^+ + 8e^- \rightarrow NH_4^+ + 3H_2O$	L-3	$CH_3OH (aq) \rightarrow CH_2O (aq) + 2H^+ + 2e^-$
E	$FeOOH (s) + HCO_3^- + 2H^+ + e^- \rightarrow FeCO_3 (s) + 2H_2O$	L-4	$CH_4 (g) + H_2O \rightarrow CH_3OH (aq) + 2H^+ + 2e^-$
F	$CH_2O (aq) + 2H^+ + 2e^- \rightarrow CH_3OH (aq)$	M	$HS^- + 4H_2O \rightarrow SO_4^{2-} + 9H^+ + 8e^-$
G	$SO_4^{2-} + 9H^+ + 8e^- \rightarrow HS^- + 4H_2O$	N	$FeCO_3 (s) + 2H_2O \rightarrow FeOOH (s) + HCO_3^- + 2H^+ + e^-$
H	$CO_2 (g) + 8H^+ + 8e^- \rightarrow CH_4 (g) + 2H_2O$	O	$NH_4^+ + 3H_2O \rightarrow NO_3^- + 10H^+ + 8e^-$
J	$N_2 (g) + 8H^+ + 6e^- \rightarrow 2NH_4^+$	P	$MnCO_3 (s) + 2H_2O \rightarrow MnO_2 (s) + HCO_3^- + 3H^+ + 3e^-$

Figure 4-10. Sequence of microbially mediated redox processes. Letters refer to reactions in Table 4-3. From *AQUATIC CHEMISTRY*, 3rd Edition by W. Stumm and J. J. Morgan. Copyright © 1996. This material is used by permission of John Wiley & Sons, Inc.



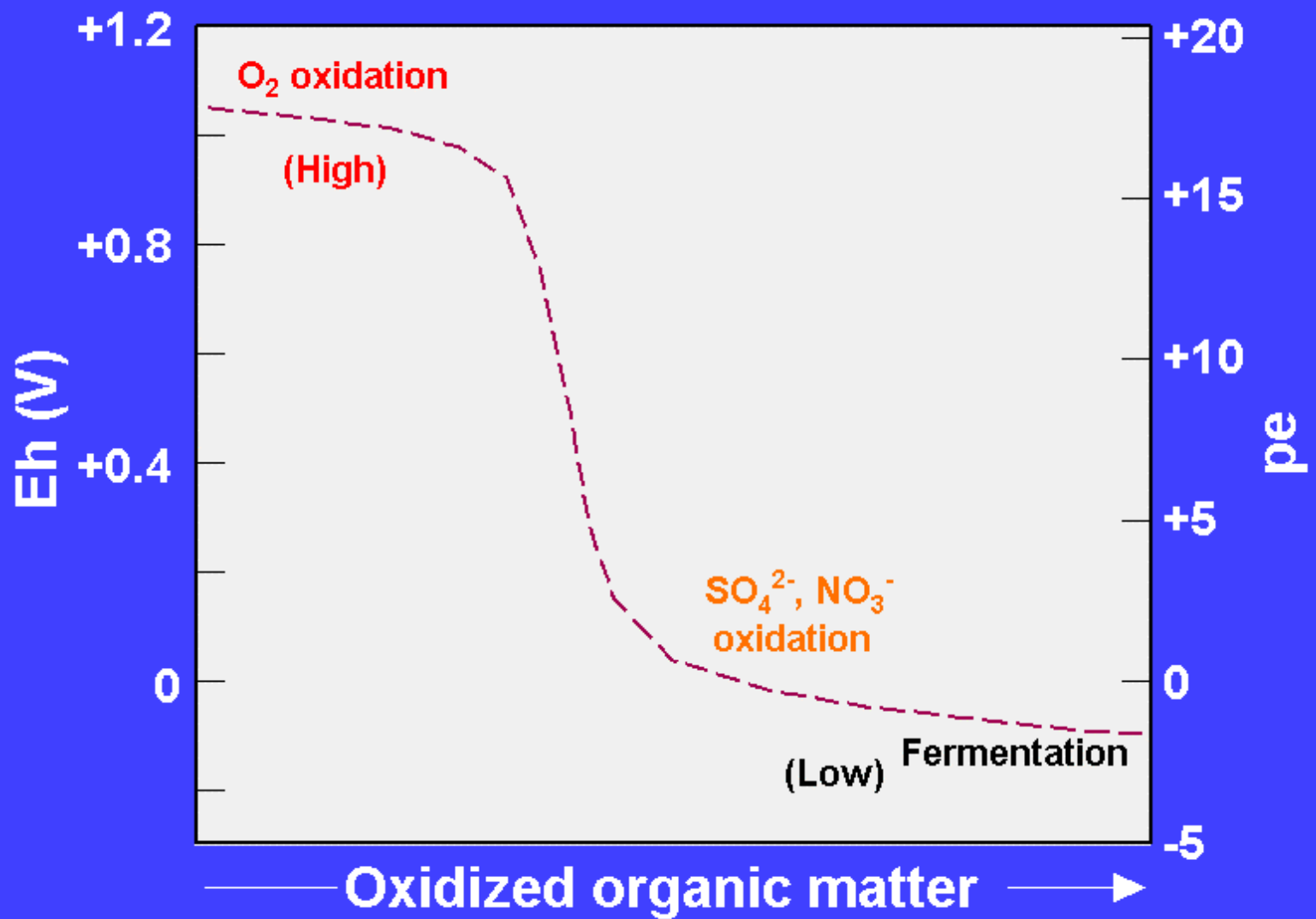


Figure 4-11. Schematic representation of redox buffering regions in acidic waters. Modified from vanLoon and Duffy (2000).

Table 4-4. Oxidation-reduction classification of natural environments

Environment	Dissolved gases (10^{-6} mol L ⁻¹)	Characteristic phases
Oxic	$O_2 > 30$	Hematite, goethite, ferrihydrite, MnO ₂ -type phases, no organic matter
Suboxic	$O_2 < 30$ and ≥ 1	Hematite, goethite, ferrihydrite, MnO ₂ -type phases, minor organic matter
Anoxic	$O_2 < 1$	
Sulfidic	$H_2S \geq 1$	Pyrite, marcasite, rhodocrosite, organic matter
Nonsulfidic	$H_2S < 1$	
Postoxic		Low-temperature Fe ²⁺ and Fe ³⁺ silicates, siderite, vivianite, rhodocrosite, no sulfide minerals, minor organic matter
Methanic		Siderite, vivianite, rhodocrosite, earlier formed sulfide minerals, organic matter

Figure 4-12. Eh ladder plot at pH = 5.7 for some of the reactions previously described in the chapter. $O_{2(g)} = 0.21$ atm, $N_{2(g)} = 0.77$ atm, activities of aqueous species = 1×10^{-3} mol L⁻¹. Numbers in parentheses refer to equations in the text.

Eh (mV)

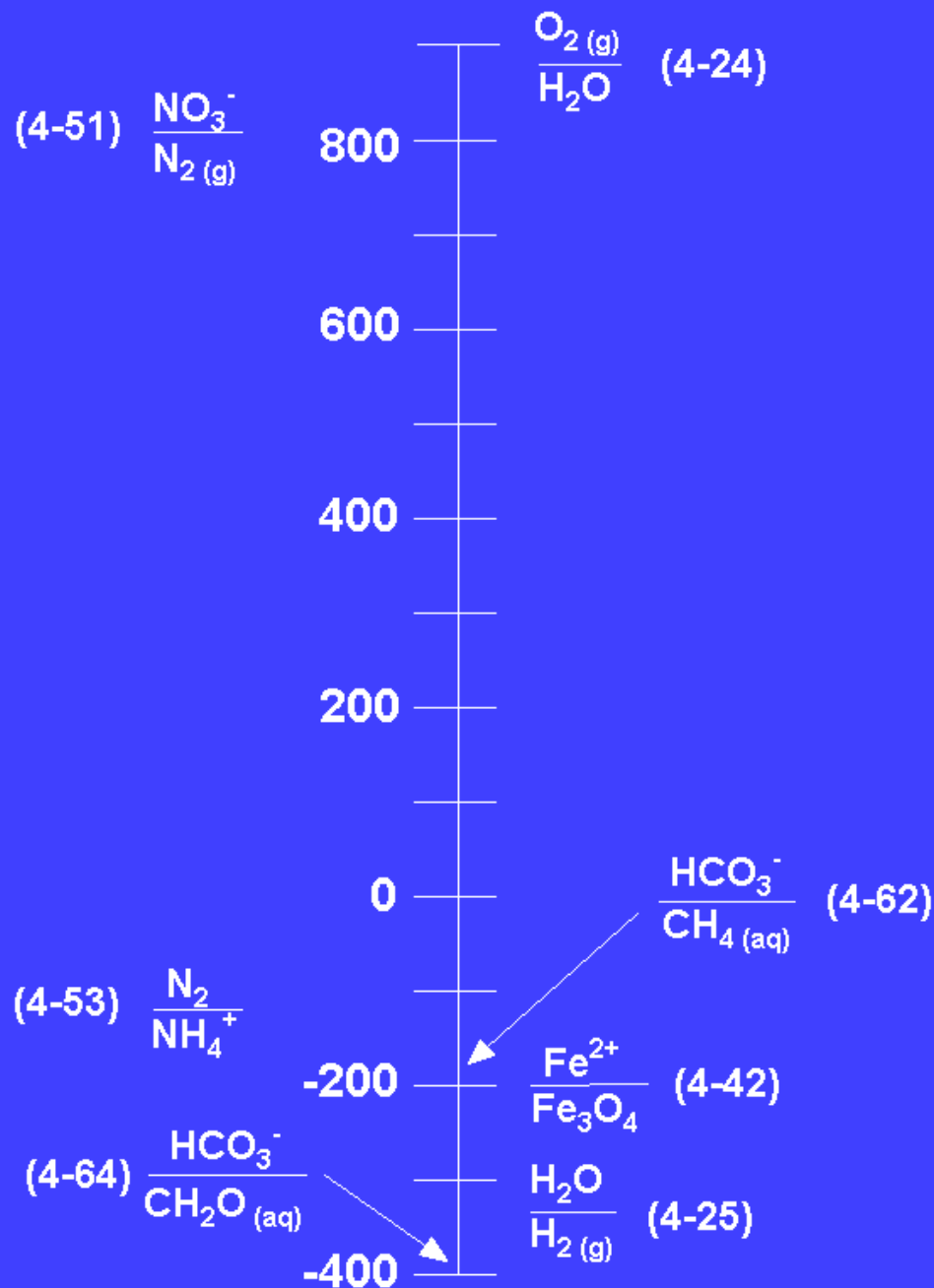
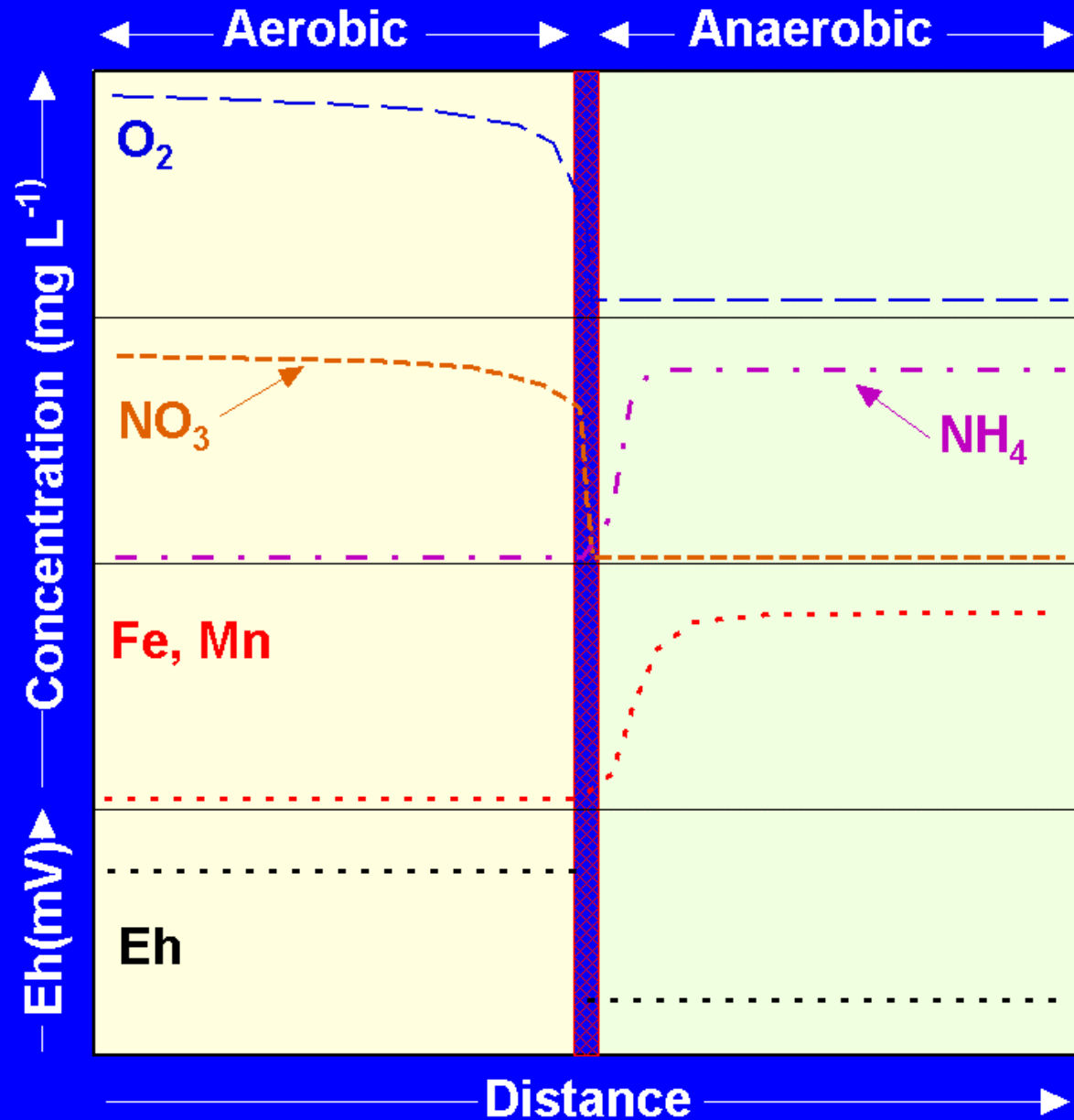


Figure 4-13. Schematic representation of changes that would occur across a redox interface between aerobic and anaerobic groundwaters.



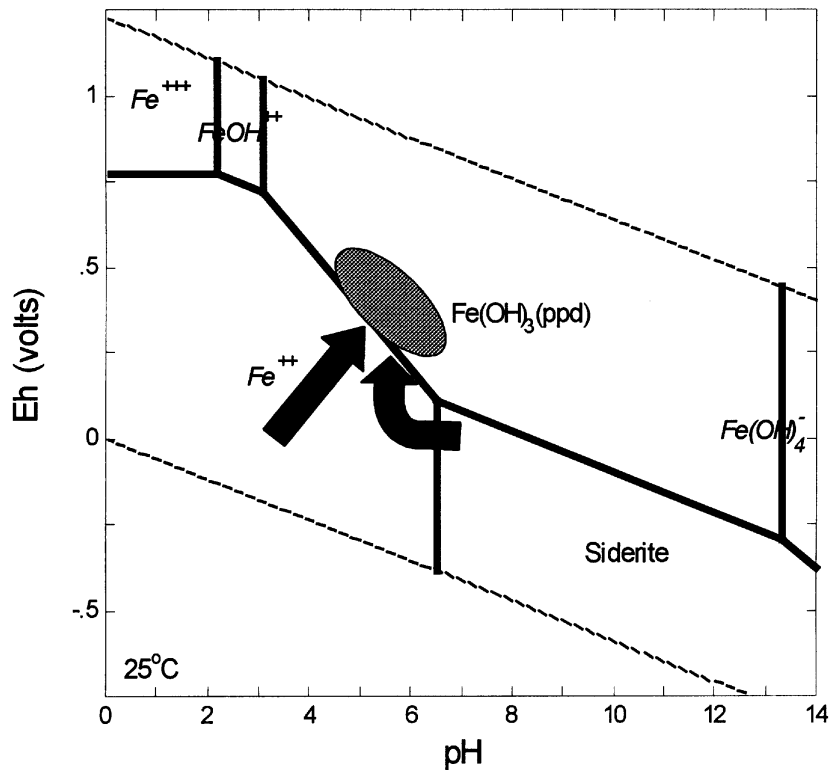


Figure 4-C1-1. Iron Eh-pH diagram at 25°C and 1.013 bars. The ellipsoidal field is the range in Eh-pH values for the spoil solution. The straight and curved arrows show hypothetical reaction paths for waters reacting with the pyritic and sideritic spoils, respectively. The spoil waters fall within the Fe-hydroxide field, and iron is apparently removed from solution as an Fe-hydroxide flocculate. Personal communication, D. Larsen, 2000.

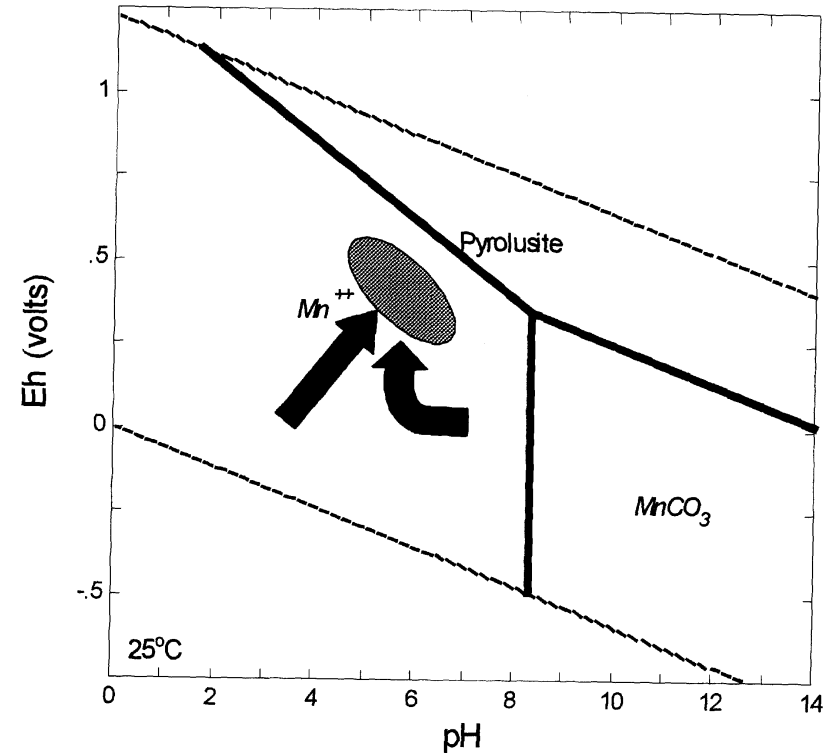
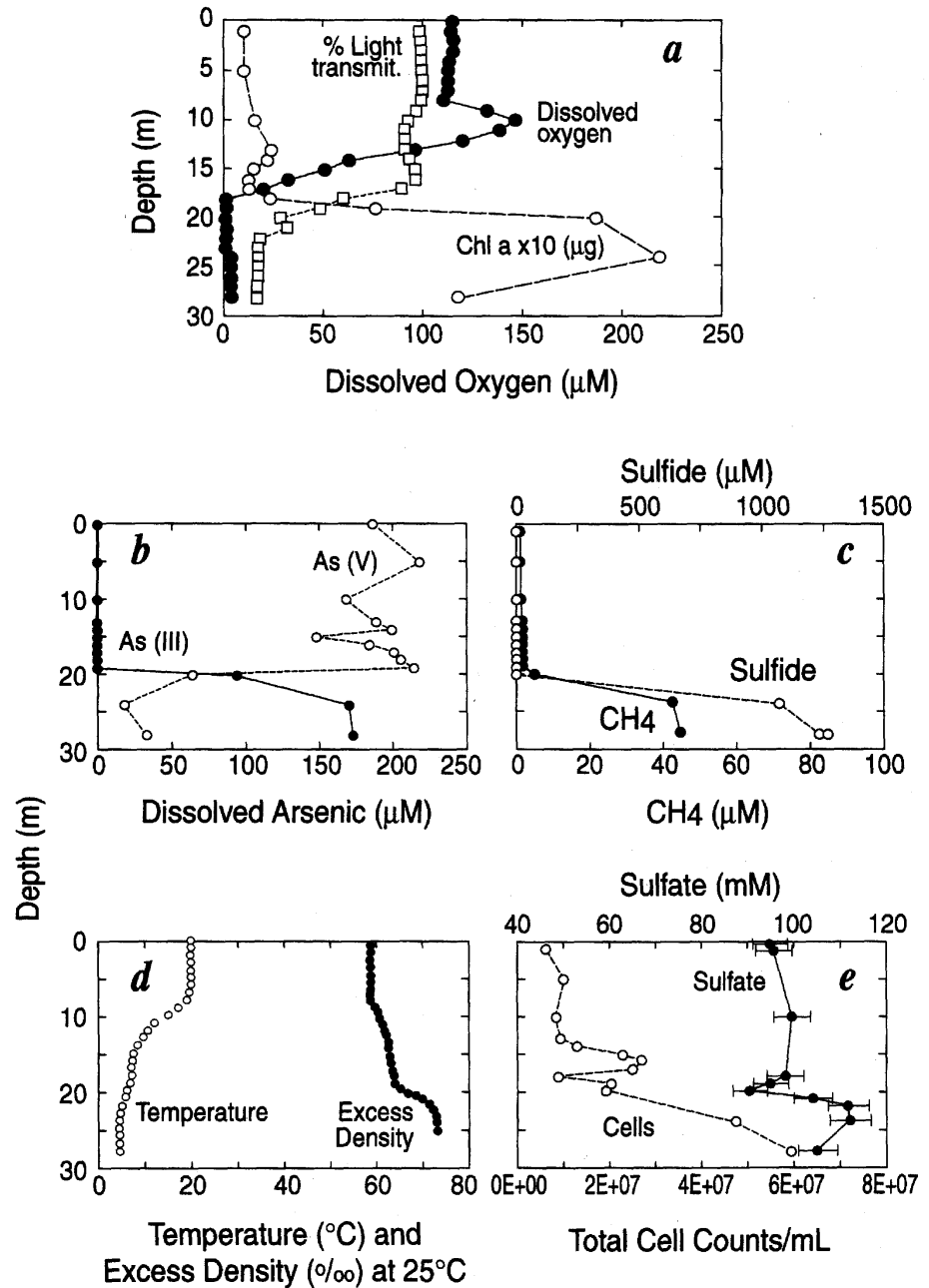


Figure 4-C1-2. Manganese Eh-pH diagram at 25°C and 1.013 bars. Field and arrows same as Figure 4-C1-1. The spoil waters fall within the Mn^{2+} field, and manganese remains in solution. If the pH and Eh were increased, the manganese would be removed from solution as a Mn-hydroxide flocculate. Personal communication, D. Larsen, 2000.

Figure 4-C2-1. Variations with depth of various physical, chemical, and biological parameters for Mon Lake in July, 1999. From Oremland et al. (2000).



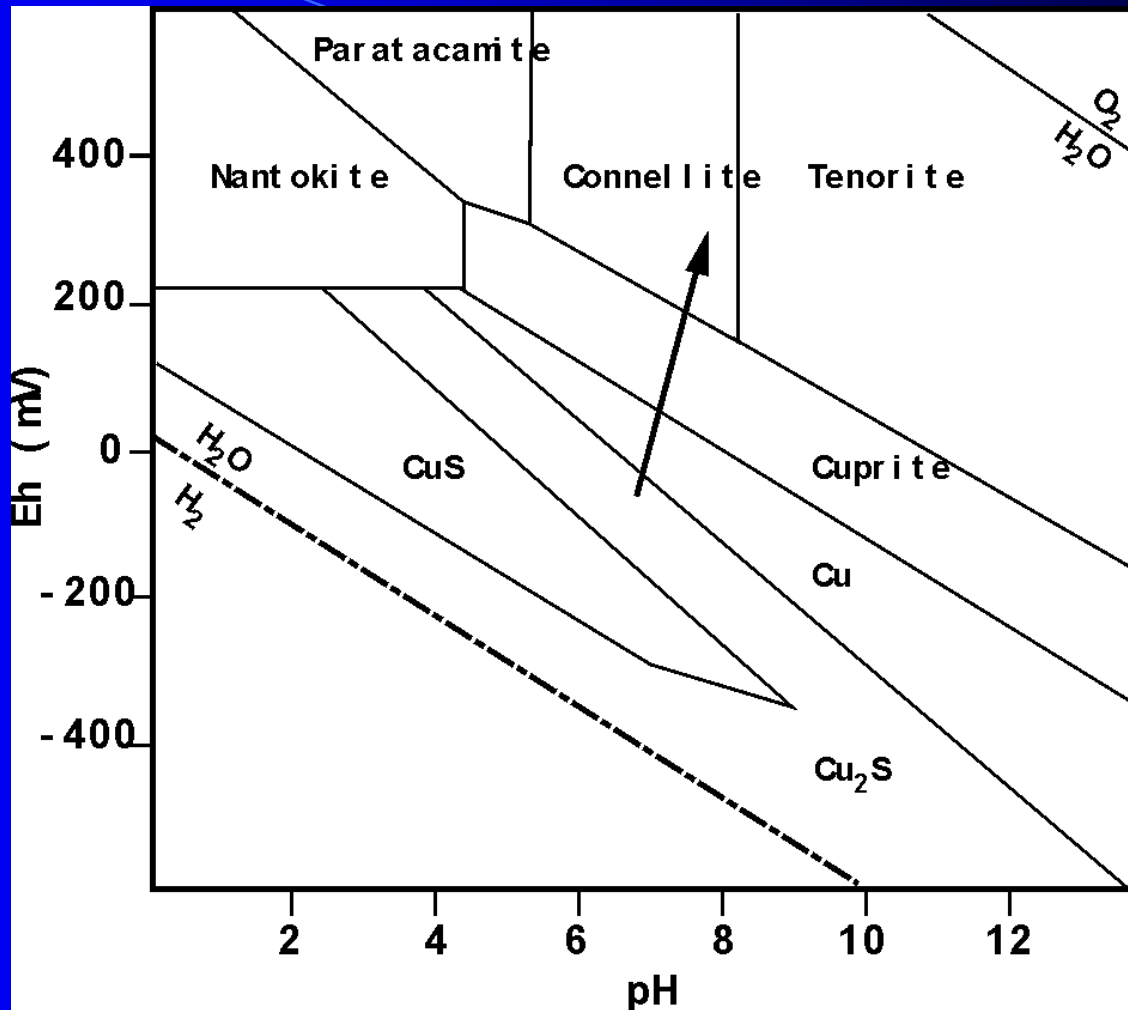


Figure 4-C4-1. Eh-pH diagram for copper. Arrow shows Eh-pH trend for redox front. From Stoffyn-Egli et al. (1998).

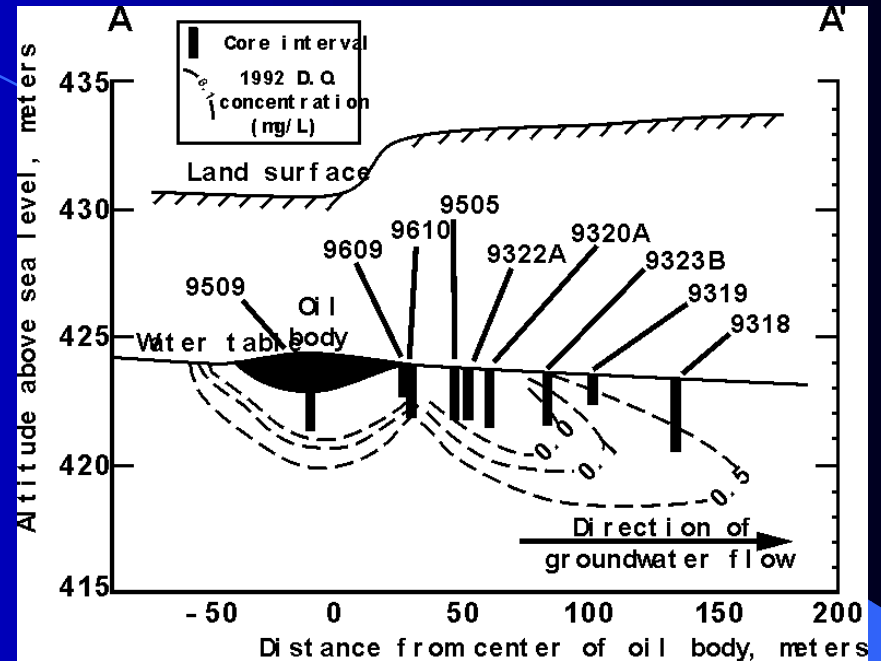
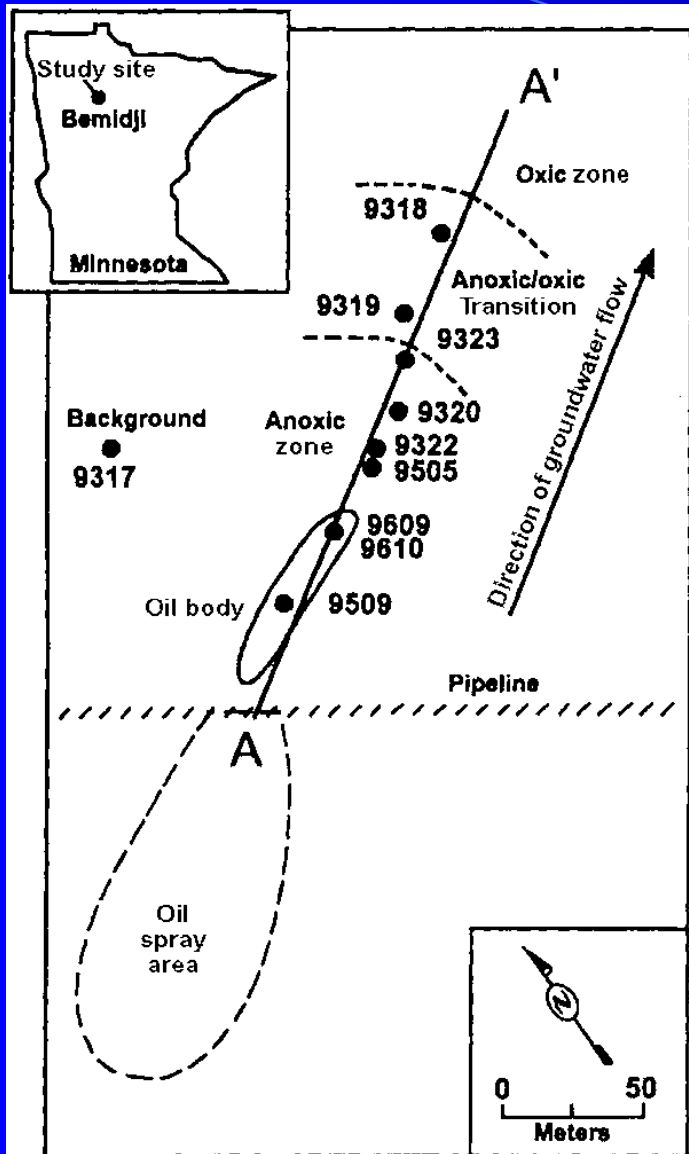


Figure 4-C6-2. Cross-section showing the extent of the anoxic plume, dissolved oxygen content, and location of core samples. From Tuccillo et al. (1999).

Figure 4-C6-1. Location of study site, redox zones, and locations of core samples. From Tuccillo et al. (1999).